Nuclear Physics B313 (1989) 541–559
North-Holland, Amsterdam

STRONG COUPLING QCD AT FINITE BARYON-NUMBER DENSITY

F. KARSCH and K.-H. MÜTTER[1]

Theory Division, CERN, CH-1211 Genève 23, Switzerland

Received 13 June 1988
(Revised 2 September 1988)

We present a new representation of the partition function for strong-coupling QCD which is suitable also for finite baryon-number-density simulations. This enables us to study the phase structure in the canonical formulation (with fixed baryon number B) as well as the grand canonical one (with fixed chemical potential μ). We find a clear signal for a first-order chiral phase transition at $\mu_c a = 0.63$. The critical baryon-number density $n_c a^3 = 0.045$ is only slightly higher than the density of nuclear matter.

1. Introduction

The phase structure of QCD at finite temperature has been studied in detail [1]. The existence of a first-order phase transition is well established. While a similar situation is expected to persist at finite baryon-number density, its numerical analysis turned out to be difficult. Both formulations of finite density QCD, the grand canonical with a non-zero chemical potential μ [2], as well as the canonical one at fixed non-zero baryon number B [3], suffer from the fact that the Boltzmann factors in the partition function are not strictly positive. This rules out the application of standard Monte Carlo techniques. Moreover, it has been shown that an analysis of finite density QCD in the quenched approximation leads to inconsistencies related to singularities of the fermion determinant [4]. A correct implementation of dynamical fermions thus seems to be mandatory*.

Some progress has been achieved in the strong-coupling limit. Here it is possible to represent the partition function as a system of monomers, dimers and baryonic loops [7]. However, the weights for the baryonic loops turn out to be positive only if the number of colours N_c is even [8]. For $N_c = 4$, the phase structure has been studied in the grand canonical formulation and a first-order chiral phase transition

[1] On leave of absence from Physics Department, University of Wuppertal, Wuppertal, FRG.

* A first attempt of a finite density calculation for the SU(3) case with the recently developed technique [5] of computing the partition function directly has been undertaken by Gocksch [6]. However, this approach seems to be limited to rather small lattices.

0550-3213/89/$03.50© Elsevier Science Publishers B.V.
(North-Holland Physics Publishing Division)

has been found at a critical value of the chemical potential μ consistent with mean-field predictions [4, 8].

It is the purpose of this paper to investigate the phase structure for strong-coupling QCD with SU(3) gauge field, staggered fermions and four flavours. In sect. 2, we review [7] how to integrate the SU(3) gauge fields. In sect. 3 the integration of the quark fields is performed. This leads to the representation of the partition function in terms of monomers, dimers and baryonic loops mentioned above. In sect. 4 we address the problem of how to handle the baryonic loops with their oscillating weights. The solution is found in a new representation of the QCD partition function as a statistical system of monomers, dimers and polymers (MDP-system). This system has strictly positive weights for $\mu = 0$ (or $B = 0$) and $r = a/a_t = 1$.

At finite density some of the Boltzmann weights will still be negative. However, as will be shown in sect. 5, the dominant contributions to the partition function have positive weights. This allows for the design of an algorithm that generates configurations distributed according to the absolute value of the Boltzmann weights. The sign of the weights can be absorbed in the observables.

The reader who is mainly interested in the physical results of our simulation should proceed immediately to sect. 6. There we show the behaviour of the chiral condensate, the baryon-number density and the energy density as a function of the chemical potential. A sharp first-order phase transition is found. The signal for this transition appears to be weaker in a simulation with canonical Boltzmann weights, i.e. at fixed baryon-number densities.

2. The SU(3) link integral

Let us start with our definitions and notations. The partition function of a system of quarks and gluons in the strong-coupling limit is given by

$$Z(2ma, \mu, r) = \int \mathrm{d}\bar{\psi}\, \mathrm{d}\psi \int \mathrm{d}U \mathrm{e}^{S_\mathrm{F}} \tag{2.1}$$

where $\bar{\psi}, \psi$ denote the quark fields and U the SU(3) gluon field. S_F is the fermion action

$$S_\mathrm{F} = \bar{\psi} \Delta \psi , \tag{2.2}$$

which couples the quark fields $\bar{\psi}, \psi$ bilinearly via the fermion matrix

$$\Delta = 2ma + \sum_{\langle xy \rangle} U(x, y) \zeta(x, y) . \tag{2.3}$$

We will use here staggered fermions. A chemical potential μ, which controls the

quark-number density of the system is incorporated via the link factor [2]*

$$\zeta(x,y)=\epsilon(x,y)\begin{cases} re^{\mu a_t}, & \text{if } (x-y)_4=1, \\ -re^{\mu a_t} & \text{if } (x-y)_4=-1, \\ \pm 1, & \text{if } (x-y)_k=\pm 1, \quad k=1,2,3. \end{cases} \tag{2.4}$$

The $\epsilon(x,y)$ are the usual signs associated with staggered fermions, $r=a/a_t$ is the ratio of the lattice spacings in space and time directions. Choosing $r\neq 1$ allows us to vary the temperature $T=1/N_t a_t$ of the system continuously.

In the absence of the gluonic part of the action the integrals over the SU(3) link variables $U(x,y)$ can be computed [7]

$$\begin{aligned} F(x,y) &= \int \mathrm{d}U \exp\left[\bar{\psi}(x)U\zeta(x,y)\psi(y)+\bar{\psi}(y)U^{\dagger}\zeta(y,x)\psi(x)\right] \\ &= 1-\tfrac{1}{3}\rho(x,y)M(x)M(y)+\tfrac{1}{12}(\rho(x,y)M(x)M(y))^2 \\ &\quad -\tfrac{1}{36}(\rho(x,y)M(x)M(y))^3+\zeta(x,y)^3\bar{B}(x)B(y)+\zeta(y,x)^3\bar{B}(y)B(x) \end{aligned} \tag{2.5}$$

The quark-field dependence can be absorbed in "meson fields"

$$M(x)=\bar{\psi}(x)\psi(x)=\sum_{a=1,2,3}\bar{\psi}_a(x)\psi_a(x)=\sum_{a=1,2,3}M_a(x), \tag{2.6}$$

and "baryon–antibaryon fields"

$$B(x)=\psi_1(x)\psi_2(x)\psi_3(x), \qquad \bar{B}(x)=\bar{\psi}_3(x)\bar{\psi}_2(x)\bar{\psi}_1(x); \tag{2.7}$$

$\rho(x,y)$ is the "mesonic" link factor

$$\rho(x,y)=\zeta(x,y)\zeta(y,x)=-\begin{cases} r^2, & \text{if } (y-x)_4=\pm 1, \\ 1, & \text{if } (y-x)_k=\pm 1, \quad k=1,2,3. \end{cases} \tag{2.8}$$

The quark fields are described by Grassmann variables with the well-known property

$$\psi_a(x)\psi_a(x)=\bar{\psi}_a(x)\bar{\psi}_a(x)=0.$$

This enables us to reduce the quadratic and cubic terms in the meson fields

* For a generalization of this prescription to introduce a chemical potential see ref. [9].

$M(x)M(y)$ to "dimer" operators

$$(M(x)M(y))^2 = (2!)^2 D_2(x, y)$$

$$= (2!)^2 (M_1(x)M_2(x) + M_1(x)M_3(x) + M_2(x)M_3(x))$$

$$\times (M_1(y)M_2(y) + M_1(y)M_3(y) + M_2(y)M_3(y)), \quad (2.9)$$

$$(M(x)M(y))^3 = (3!)^2 D_3(x, y)$$

$$= (3!)^2 M_1(x)M_2(x)M_3(x)M_1(y)M_2(y)M_3(y). \quad (2.10)$$

For convenience we also introduce a third dimer operator

$$D_1(x) = (M_1(x) + M_2(x) + M_3(x))(M_1(y) + M_2(y) + M_3(y)). \quad (2.11)$$

In terms of the dimer operators the link integral acquires the form

$$F(x, y) = 1 - \tfrac{1}{3}\rho(x, y)D_1(x, y) + \tfrac{1}{3}\rho(x, y)^2 D_2(x, y) + -\rho(x, y)^3 D_3(x, y)$$

$$+ \zeta(x, y)^3 \bar{B}(x)B(y) + \zeta(y, x)^3 \bar{B}(y)B(x). \quad (2.12)$$

3. Monomers, dimers, baryon loops

In this section, we will compute the partition function (2.1) making use of eq. (2.12) for the link integral

$$Z = \int d\bar{\psi}\, d\psi \exp\left[2ma \sum_x M(x)\right] \prod_{\langle xy \rangle} F(x, y). \quad (3.1)$$

Non-vanishing contributions to the integrals over the quark fields are obtained only if each site x of the lattice is occupied: either by three mesons, $M_1(x)M_2(x)M_3(x)$; or by a baryon–antibaryon pair, $\bar{B}(x)B(x)$.

As will be shown below, this rule generates geometrical patterns on the lattice, which are built up from "monomers", "dimers" and "baryonic loops".

(a) Monomers live on sites x. They carry a weight $2ma$ and they are generated by the mass term

$$\exp[2maM(x)] = 1 + 2ma(M_1(x) + M_2(x) + M_3(x))$$

$$+ (2ma)^2 (M_1(x)M_2(x) + M_1(x)M_3(x) + M_2(x)M_3(x))$$

$$+ (2ma)^3 M_1(x)M_2(x)M_3(x). \quad (3.2)$$

For SU(3), the monomer occupation number $n_M(x)$ at site x takes the values

$$n_M(x) = 0, 1, 2, 3. \tag{3.3}$$

The total number of monomers is denoted by

$$N_M = \sum_x n_M(x). \tag{3.4}$$

(b) Dimers live on links $\langle xy \rangle$. There are three types of them, which we discriminate by the number $n_D(x, y)$ of dimer lines connecting the neighbouring sites x and y

$$\begin{array}{lccc} & x - - - y & x = = = y & x \equiv \equiv \equiv y \\ n_D(x, y) = & 1 & 2 & 3 \\ w(x, y) = & \frac{1}{3}\rho(x, y) & \frac{1}{3}\rho(x, y)^2 & \rho(x, y)^3 \end{array}. \tag{3.5}$$

The weights of the type j dimers ($j = 1, 2, 3$) are given in the last line. Type j dimers are generated by the dimer operator D_j (cf. eqs. (2.9)–(2.11)).

(c) Baryonic loops are self-avoiding. They are generated by a product of baryon–antibaryon operators $\bar{B}(x)B(y)$ along the loop C

$$\prod_{\langle xy \rangle \in C_+} \bar{B}(x)B(y).$$

By the subscript $\pm$ at C, we denote the orientation of the loop clockwise (C_-) and counterclockwise (C_+), respectively. A baryonic loop is accompanied by a weight factor

$$\rho(C) = -\prod_{\langle xy \rangle \in C_+} \zeta(x, y)^3 - \prod_{\langle xy \rangle \in C_-} \zeta(x, y)^3 \tag{3.6}$$

Next we put these objects on the lattice with the following rules.

(1) Baryonic loops are isolated objects. Each site x, occupied by a baryonic loop, carries a baryon–antibaryon pair and therefore cannot carry any further object.

(2) All remaining sites x have to be occupied with three mesons $M_1(x)M_2(x)M_3(x)$.

This means that the number $n_D(x)$ of dimer lines ending in x plus the number $n_M(x)$ of monomers in x has to be three

$$n_D(x) + n_M(x) = 3. \tag{3.7}$$

Moreover, we need at each site x one meson of each type: M_1, M_2, M_3. This rule

TABLE 1
The weights $w(x)$ at site x as they depend on the node types 0 to 6

node type	0	1	2	3	4	5	6
$n_D(x)$	3	2	1	0	2	3	3
$n_M(x)$	0	1	2	3	1	0	0
$w(x)$	3	6	3	1	3	6	1

defines the weights $w(x)(2ma)^{n_M(x)}$ carried by each site which can be read off table 1.

The partition function (3.1) can finally be written as a sum over monomer–dimer loop configurations K

$$Z(2ma, r, \mu) = \sum_K w_K , \tag{3.8}$$

where the weight w_K is determined by the site, link, and loop weights, specified above

$$w_K = (2ma)^{N_M} \prod_x w(x) \prod_l w(l) \prod_C \rho(C) . \tag{3.9}$$

A typical configuration is shown in fig. 1.

4. Eliminating the baryon loops: The monomer–dimer–polymer system

As it stands, the monomer, dimer, baryon-loop representation (3.8) of the partition function is not suitable for a simulation, since the baryon-loop weights $\rho(C)$ (cf. eq. (3.9)) are not positive definite.

For Wilson loops C, $\rho(C)$ turns out to be

$$\rho(C) = 2\sigma(C) r^{3N_t(C)} , \tag{4.1}$$

$$\sigma(C) = -(-1)^{N_t(C)} \prod_{\langle x,y \rangle \in C} \epsilon(x, y) , \tag{4.2}$$

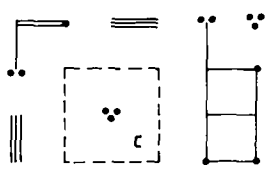

Fig. 1. A typical monomer-dimer baryon-loop configuration. The baryon loop is indicated as a dashed line.

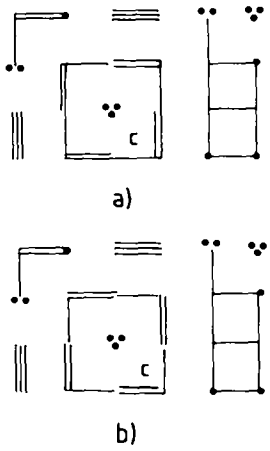

Fig. 2. Same as fig. 1 with the baryon loop replaced by a chain of type 1-type 2 dimers (polymer). There are two possibilities for such a replacement. The first one is shown in (a), the second in (b).

$N_-(C)$ and $N_t(C)$ are the number of links on C in the negative direction and in the (positive or negative) time direction, respectively.

For Polyakov loops C_k, winding around the lattice k-times in the time direction, we find

$$\rho(C_k) = \sigma(C_k) r^{3N_t(C_k)} \cosh(3k\mu/T), \tag{4.3}$$

$$\sigma(C_k) = -(-1)^{k-N_t(C_k)} \prod_{\langle x,y\rangle \in C_k} \epsilon(x,y); \tag{4.4}$$

N_t is the number of sites in time direction and μ is the chemical potential. In the following, we will call Wilson loops C and Polyakov loops C_k positive (negative), if*

$$\sigma(C) = \pm 1, \qquad \sigma(C_k) = \pm 1.$$

The sign of a loop only depends on its geometry. Some examples are shown in fig. 3.

We now address the crucial question of how to deal with negative baryon loops in a simulation. The following observation will be helpful. We can associate to each configuration with one baryon loop (like the one shown in fig. 1) two "pure monomer-dimer" configurations, as shown in figs. 2a, b. There, we have substituted the baryon loop of fig. 1 by a chain of type 1-type 2 dimers following C. We call such a chain a polymer. Instead of summing over the three configurations in figs. 1, 2a, 2b, we can consider as well the sum of the pure monomer-dimer configurations

* The different overall sign for Wilson and Polyakov loops originates from the antiperiodic boundary conditions in the time direction.

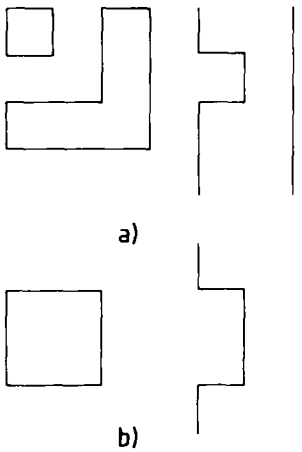

Fig. 3. Typical forms of selfavoiding loops: (a) with positive sign $\sigma(C) = 1$; (b) with negative sign $\sigma(C) = -1$.

of figs. 2a, b, but with a new weight for the polymer C

$$r^{2N_{Dt}(C)}w(C) = r^{2N_{Dt}(C)}\left(1 + r^{n_t(C)}\sigma(C)\right), \tag{4.5}$$

where

$$n_t(C) = 3N_t(C) - 2N_{Dt}(C) = 0, \pm 2. \tag{4.6}$$

Here, $N_{Dt}(C)$ is the number of dimer lines in the time direction on the polymer C. Note, that for a negative loop ($\sigma(C) = -1$) eq. (4.5) is zero, if either $r = a/a_t = 1$ or $n_t(C) = 0$. The latter is the case for all loops with a number of links in the time direction, which is a multiple of four.

In a quite analogous fashion we can associate to each configuration with a baryonic Polyakov loop C_k, two pure monomer–dimer configurations with a polymer along C_k carrying a weight

$$r^{2N_t(C_k)}w(C_k) = r^{2N_t(C_k)}\left(1 + \sigma(C_k)\cosh(3k\mu/T)\right). \tag{4.7}$$

For negative Polyakov loops C_k, $\sigma(C_k) = -1$, this weight is zero if $\mu = 0$.

It is now straightforward to map the monomer–dimer baryon-loop system onto a monomer-dimer-polymer (MDP) system with partition function

$$Z(2ma, \mu, r) = \sum_K w_K,$$

and a weight for the MDP configuration K

$$w_K = (2ma)^{N_M} r^{2N_{Dt}} (1/3)^{N_{D1}+N_{D2}} \prod_x w(x) \prod_C w(C), \tag{4.8}$$

where N_M, N_{Dt} and N_{Dj}, $j = 1,2$ are the numbers of monomers and dimer lines in the time direction and type j dimers, respectively. The equivalence of the monomer–dimer baryon system and the MDP system is obvious for $r = 1$. Each polymer carries a weight 1 in the monomer–dimer baryon-loop system and a weight $[1 + \sigma(C)]$ in the MDP system. The additional contribution $\sigma(C)$ is just half of the baryon-loop contribution. Therefore, by construction the partition functions with weights given by eq. (3.9) and eq. (4.8) are equal*.

In the transition region to a quark–gluon plasma the quantities of physical interest are the chiral condensate $\langle\bar{\psi}\psi\rangle$, the baryon-number density n and the internal energy density ϵ. In the strong-coupling limit – considered in this paper – these quantities can be easily measured, making use of the equivalence of the quark–gluon system to the monomer–dimer–polymer (MDP) system

(a) The chiral condensate $\langle\bar{\psi}\psi\rangle$ is obtained from the monomer density $V^{-1}\langle N_M\rangle$

$$\langle\bar{\psi}\psi\rangle = V^{-1} \frac{\partial}{\partial 2ma} \log Z(2ma, \mu a_t, r) = (2maV)^{-1} \langle N_M\rangle . \tag{4.9}$$

(b) The baryon-number density n can be extracted from the density $V^{-1}\langle N(C_k)\rangle$ of polymers C_k (winding around the lattice k times in the time direction)

$$n = (3VN_t)^{-1} \frac{\partial}{\partial \mu a_t} \log Z(2ma, \mu a_t, r)$$

$$= (3VN_t)^{-1} \sum_{C_k} \frac{\partial}{\partial \mu a_t} \log w(C_k) \langle N(C_k)\rangle . \tag{4.10}$$

(c) The internal energy density ϵ_μ is determined by the average number of dimer lines in the time direction $\langle N_{Dt}\rangle$ and the average numbers $\langle N(n_t(C) = \pm 2,$

* In principle one can map the baryon loop C also onto other dimer configurations which have the same geometry and are "isolated" as the baryon loop C, e.g. chains of type-three dimers. However, with this prescription, the resulting new weights, including the baryon-loop contributions, become very complicated, if the type-three dimers cluster in such a way, that different occupations with self-avoiding loops are possible. This problem does not occur with the mapping of baryon loops onto polymers.

$\sigma(C) = \pm 1)\rangle$ of polymers C with fixed $n_t(C) = \pm 2$ and $\sigma = \pm 1$

$$\epsilon_\mu = -(VN_t)^{-1} \frac{\partial}{\partial a_t} \log Z(2ma, \mu a_t, r = a/a_t)$$

$$= 2(VN_t a_t)^{-1} \Big[\langle N_{Dt} \rangle + (1+r^2)^{-1} \langle N(2,1) \rangle - (1+r^{-2})^{-1} \langle N(-2,1) \rangle$$

$$- (1-r^2)^{-1} \langle N(2,-1) \rangle + (1-r^{-2})^{-1} \langle N(-2,-1) \rangle \Big] . \quad (4.11)$$

The derivative in eq. (4.11) has to be taken at fixed fugacity, i.e. fixed μa_t. We note that on an isotropic lattice, $r = 1$, only the first term in eq. (4.11) contributes. All other contributions add up to zero.

Eqs. (4.9) and (4.11) yield the chiral condensate and the internal energy for fixed chemical potential μ, i.e. in the grand canonical ensemble. The above quantities can also be studied in a canonical ensemble, i.e. at fixed baryon number B. As was shown in ref. [3], the canonical partition function $Z(T, B)$ with fixed baryon number B, can be computed from the grand canonical partition function with imaginary chemical potential $\bar{\mu} = \frac{1}{3} iT\phi$

$$Z(T, B) = (2\pi)^{-1} \int_0^{2\pi} d\phi \exp(-iB\phi) Z(T, \bar{\mu}) . \quad (4.12)$$

Therefore, we have to substitute in eq. (4.8) the weights for the N_{k+} (N_{k-}) positive (negative) Polyakov loops C_k (cf. eq. (4.7)

$$\prod_{C_k} w(C_k) = \prod_k (1 + \cosh(3k\mu/T))^{N_{k+}} \cdot (1 - \cosh(3k\mu/T))^{N_{k-}} , \quad (4.13)$$

by its Fourier projection on states with definite baryon number B

$$w_B[N_{1+}, N_{1-}, \ldots] = (2\pi)^{-1} \int_0^{2\pi} d\phi \exp(-iB\phi)$$

$$\times \prod_k (1 + \cos k\phi)^{N_{k+}} \cdot (1 - \cos k\phi)^{N_{k-}} . \quad (4.14)$$

These weights have a simple form for configurations which contain only Polyakov loops C_1 with winding number 1. In this case the weight turns out to be

$$w_B[N_{1+}, N_{1-}] = \frac{(-1)^{N_{1-}}}{4^{N_{1+}+N_{1-}}} \sum_{k=0}^{2N_{1-}} (-1)^k \binom{2N_{1-}}{k} \binom{2N_{1+}}{N_{1+} + N_{1-} - k - B} . \quad (4.15)$$

In fact only these type of configurations showed up in our simulation of the MDP system at fixed baryon number.

5. The simulation of the MDP system

The Boltzmann weights in the MDP system, as they are given by eqs. (4.7) and (4.8) are non-negative for $\mu = 0$ and $r = 1$. For $\mu > 0$, configurations with negative weights can occur, if the type-1–type-2 dimers create an odd number of polymers along negative Polyakov loops C_k. A typical example of such a loop is shown in fig. 3b.

We can associate to each configuration K a sign σ_K. In our simulation, we will perform the update with positive Boltzmann weight $|w_K|$. Let us denote averages of observables O with positive weight by $\langle O \rangle_+$. The quantity in which we are interested is $\langle O \rangle$, the average weighted with w_K. The latter can be computed from

$$\langle O \rangle = \frac{\langle \sigma_K O \rangle_+}{\langle \sigma_K \rangle_+}, \tag{5.1}$$

if the average sign $\langle \sigma_K \rangle_+$ of the configurations turns out to be non-zero.

Previous attempts to simulate the full QCD partition function for $\mu \neq 0$ failed just for this reason [10]; the rapid oscillations of the sign of the Boltzmann weights could not be controlled with sufficient accuracy. Moreover, cancellations between positive and negative contributions were extremely important as zeros of the fermion determinant had to cancel poles in the fermion propagators [11]. In the present case we expect to be in a much better situation for two reasons. Firstly, of all the gauge fields have been integrated out exactly in the strong coupling limit – and with them a large part of the oscillations are already gone. The remaining oscillations do not seem to play an important role and are mainly of geometrical origin. Secondly, by handling the baryonic loops in the way discussed in sect. 4 we create a system that still allows for configurations with negative weights. However, at least in important limiting cases it is easy to see that the dominant contributions arise from configurations with only positive weights. The important point here is that the leading contribution at $\mu \neq 0$ comes from loops of minimal length, i.e. Polyakov loops of length N_t. These loops have positive weights. In addition the weights are strictly non-negative for the important limiting cases $\mu \to 0$ an $\mu \to \infty$.

Thus, there is some hope that an algorithm based on the MDP representation of the strong-coupling partition function can handle the remaining fluctuating signs of the Boltzmann factors. Of course, as this is a global factor, we expect the performance of any algorithm to become worse with increasing lattice size. Results from simulations on 4^4 and $8^3 4$ lattices for $ma = 0.1$, $r = a/a_t = 1$ and various values of μa are shown in fig. 4a. Indeed we observe a drop in $\langle \sigma_K \rangle$ with increasing lattice

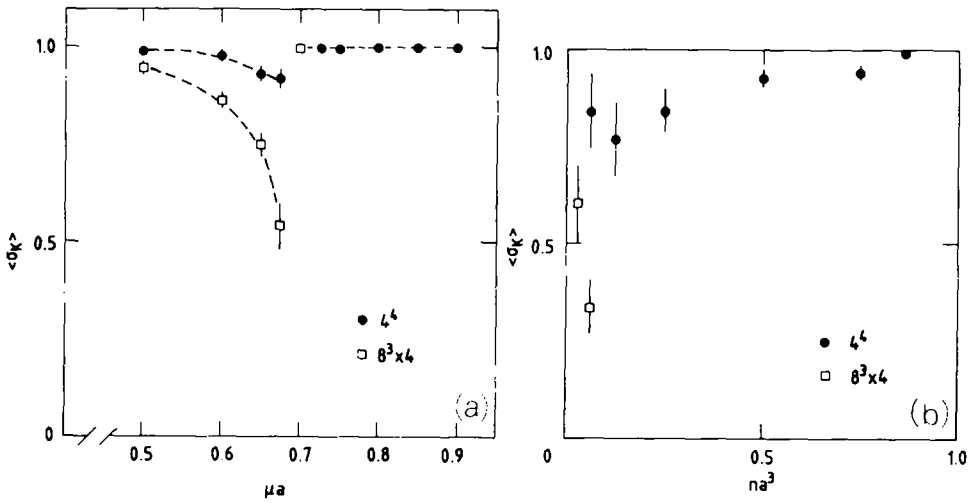

Fig. 4. The average sign of the Boltzmann weights on lattices of size 4^4 (●) and $8^3 4$ (□) in the grand canonical (a) and canonical (b) ensemble.

size. As expected $\langle \sigma_K \rangle$ approaches one in the limiting cases $\mu \to 0$ and $\mu \to \infty$. It has a minimum at the critical value μ_c.

The algorithm thus seems to work quite well on lattices of this size. A detailed presentation of results will be given in sect. 6. Let us here briefly discuss the actual algorithm used to simulate the MDP partition function. Starting from a given configuration of monomers and dimers we try to update a given link in the lattice either by replacing two monomers by a dimer or a dimer by two monomers. Of course this is not always possible; a given link has to be occupied either by a dimer or the two sites connected by the link have to be occupied by monomers. A conflicting situation occurs, if both of the above cases are true. In order to handle these cases and ensure detailed balance we define a transition matrix, which for every given (site, link) occupation suggests a unique new configuration. This configuration is then accepted or rejected according to the standard Metropolis algorithm. The possible, allowed transitions are given in table 2.

We found that in a typical configuration the fraction of links that could be updated was always between 30% and 50%, depending on the value of the quark mass and to a smaller extent also on the chemical potential. Although it is difficult to prove ergodicity for our algorithm, we think it is flexible enough to create all possible configurations.

The acceptance rate in the Metropolis part of the update, of course, depends strongly on ma and μa. It varies between 20% and 60% for $0.1 < ma < 0.7$ and $\mu < \mu_c$, but drops to less than 1% for $\mu > \mu_c$. This is related to the exponentially large weights in this case. We note, however, that updates of the lattice involve only

TABLE 2
Transition matrix between new and old configurations. All other occupations of sites and links do not lead to allowed transitions. The numbers denote the node type on the site (cf. table 1) and the dimer lines on the link connecting site 1 and 2.

old configuration			⇔	new configuration		
site 1	site 2	link	⇔	site 1	site 2	link
0	0	1	⇔	4	4	0
0	0	2	⇔	1	1	1
1	0	1	⇔	2	4	0
2	0	1	⇔	3	4	0
4	0	2	⇔	2	1	1
5	0	1	⇔	1	4	0
1	1	0	⇔	5	5	1
2	1	0	⇔	1	5	1
3	1	0	⇔	2	5	1
2	2	1	⇔	3	3	0
4	4	2	⇔	6	6	3
4	4	0	⇔	0	0	1
1	1	1	⇔	0	0	2
4	2	0	⇔	0	1	1
4	3	0	⇔	0	2	1
4	1	0	⇔	0	5	1
5	5	1	⇔	1	1	0
5	1	1	⇔	1	2	0
5	2	1	⇔	1	3	0
3	3	0	⇔	2	2	1
6	6	3	⇔	4	4	2
3	2	0	⇔	2	1	1
2	1	1	⇔	3	2	0

simple integer operations and are thus very fast. In typical simulations on a $8^3 4$ lattice we thus could easily perform several million updates per parameter set.

The situation is similar for the MDP system at finite baryon number. In fig. 4b we show the average sign of the configurations for $ma = 0.1$ as a function of the baryon number density $n = B/V$.

6. Numerical results

It has been shown that QCD at finite temperature undergoes a first-order chiral phase transition [1]. The same is expected to happen at finite baryon-number density. So far this could only be studied in the strong-coupling limit by mean-field techniques [8] or numerical simulations for SU(N_c), with N_c even. In fact, simulations for SU(4) [8] have shown that the numerical results agree quite well with mean-field predictions.

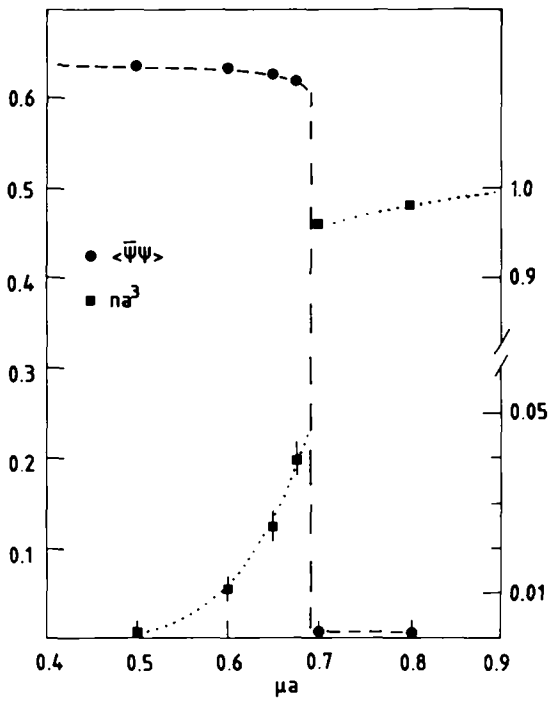

Fig. 5. The chiral condensate $\langle\bar{\psi}\psi\rangle$ and baryon number density na^3 versus μa obtained from simulations on a $8^3 4$ lattice. Lines are drawn to guide the eye. Note the change of scale for na^3 below and above the critical point.

Using the MDP algorithm, described in sect. 5, we have studied the chiral phase transition for strong-coupling QCD, i.e. with SU(3)-gauge fields and 4 light quark flavours. We find a signal for a strong first-order chiral transition. Results for the chiral condensate and the baryon-number density are shown in fig. 5 for our smallest quark mass $ma = 0.1$. Data points on this figure are based on $(2\ 4) \times 10^6$ iterations on a $8^3 4$ lattice. Observables have been calculated according to eq. (5.1) on blocks of 200 000 iterations. Errors have then been determined as statistical from these blocked measurements. Simulations with the same parameters have been performed on a 4^4 lattice. No significant size effects have been found. From this we can deduce the critical baryon-number density at the transition point. We find for $ma = 0.1$

$$\mu_c a = 0.69 \pm 0.015\,, \qquad n_c a^3 = 0.045 \pm 0.005\,. \tag{6.1}$$

The quark-mass dependence of the critical parameters has been studied by us in detail on the 4^4 lattice. Fig. 6 shows the phase diagram in the ma–μa plane. As can be seen, it agrees quite well with mean-field predictions [4, 12]. In fig. 7 we show the

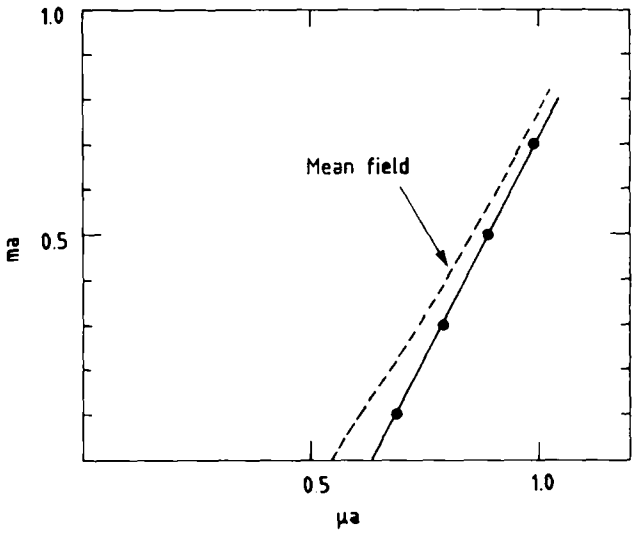

Fig. 6. Quark-mass dependence of the critical chemical potential obtained from simulations on a 4^4 lattice. The mean-field prediction of ref. [4] is also shown.

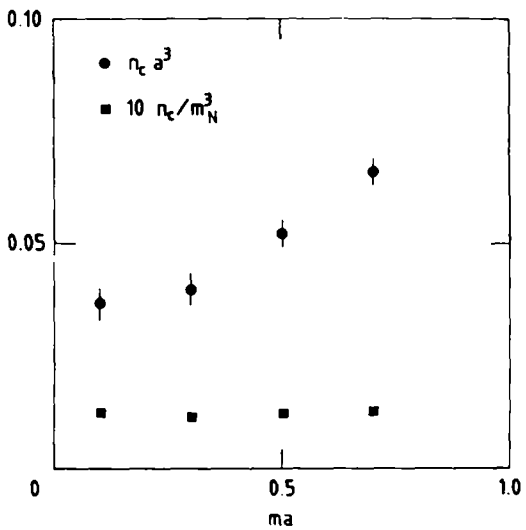

Fig. 7. Quark-mass dependence of the critical baryon-number density $n_c a^3$ obtained from simulations on a 4^4 lattice. The critical density in units of the nucleon mass is also shown.

dependence of the critical density as a function of ma. The critical density decreases in units of the lattice spacing when the quark mass is lowered. However, it stays roughly constant if we eliminate the lattice spacing in favour of the strong-coupling nucleon mass [13]

$$m_N a = \ln\left[\tfrac{1}{2}c^3 + \sqrt{1 + \tfrac{1}{8}c^6}\right], \tag{6.2}$$

$$c = m + \sqrt{8 + m^2}\,. \tag{6.3}$$

In the chiral limit we find from fig. 6 the critical chemical potential, $\mu_c a = 0.63 \pm 0.02$. Using eqs. (6.2) and (6.3) we can express this and the critical density in units of the strong coupling nucleon mass

$$\mu_c = 0.21 m_N\,, \qquad n_c = (0.0017 \pm 0.0002) m_N^3\,. \tag{6.4}$$

Though we are here in the strong-coupling limit ($\beta = 0$) and therefore far away from the continuum limit, a comparison with the yet unknown critical values in the continuum theory might nevertheless be instructive. For this purpose we replace the strong-coupling nucleon mass by the physical one*. This gives for the critical parameters in physical units

$$\mu_c \simeq 200 \text{ MeV}\,, \qquad n_c = (0.22 \pm 0.02) \text{ fm}^{-3}\,.$$

Notice that the critical density is only slightly larger than that to ordinary nuclear matter, $n_0 = 0.17/\text{fm}^3$. We have also calculated the energy per baryon, which in the broken phase turns out to be close to the nucleon mass

$$E/B = n^{-1}(\epsilon_\mu - \epsilon_0) = 3 \qquad \text{for} \quad \mu < \mu_c\,. \tag{6.5}$$

While the parameter of that broken phase up to the critical point looks quite reasonable, the nature of the symmetric phase is quite obscure in the strong-coupling limit. Immediately after the transition the number density saturates the maximal value possible on a lattice, i.e. one baryon per site. In addition the energy density drops across the transition, $E/B = 2.25$ for $\mu > \mu_c$.

In order to understand the chiral transition in the strong-coupling limit better, it would be helpful to study the properties of the system in a mixed phase. This can be achieved by fixing the baryon number rather than the chemical potential [3]. In the framework of the MDP representation this requires only a minor modification of the Boltzmann weights, as discussed in sect. 4. The signal for the phase transition, however, becomes weaker in this case. The strong first-order signal shown in fig. 5

* In other words, we fix the lattice cut-off a using the physical nucleon mass as input. Using this scale, the effective temperature for our lattices with $N_t = 4$ is $T = 83$ MeV.

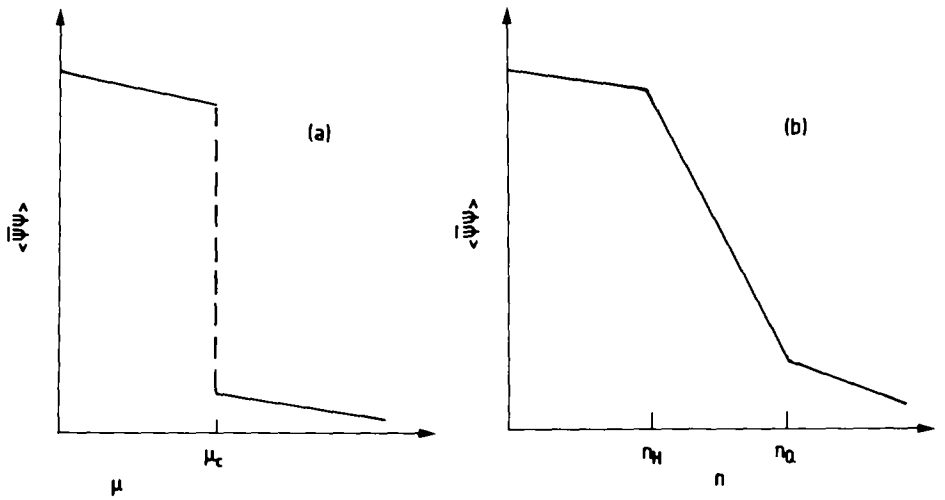

Fig. 8. Schematic behaviour of the chiral condensate $\langle\bar{\psi}\psi\rangle$ in the grand canonical (a) and canonical (b) ensemble. A first-order phase transition leads to discontinuity of $\langle\bar{\psi}\psi\rangle$ at μ_c in the grand canonical picture, whereas it only yields discontinuities in the slope of $\langle\bar{\psi}\psi\rangle$ at the onset (n_H) and end (n_Q) of the mixed phase in the canonical ensemble.

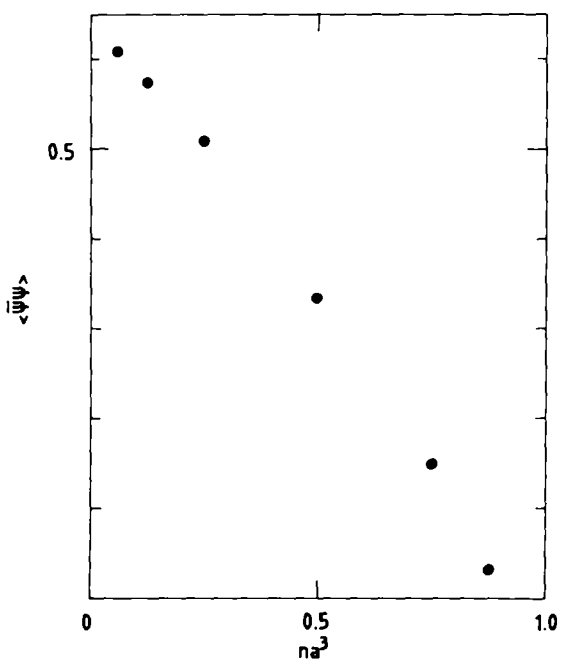

Fig. 9. $\langle\bar{\psi}\psi\rangle$ versus na^3. Results from simulations at fixed baryon number on a 4^4 lattice. Each data point is based on 2×10^6 iterations. Errors are of the size of the symbols.

at finite μ transforms into two cusps at non-zero baryon number B. The expected dependence of $\langle\bar{\psi}\psi\rangle$ as a function of n is shown schematically in fig. 8. Onset and end of the mixed phase leads to cusps rather than to discontinuities as in the grand canonical ensemble. Restoration of chiral symmetry is completed only at the end of the mixed phase.

In fig. 9 we show results for $\langle\bar{\psi}\psi\rangle$ from a simulation on a 4^4 lattice in the entire density regime. Like in the $\mu \neq 0$ simulations, we find that the mixed phase essentially covers the whole region from $na^3 = 0$ up to $na^3 = 1$. A detailed study of the low-density region on a 6^34 lattice is shown in fig. 10. For comparison, we also present some data from our $\mu \neq 0$ simulation. This demonstrates the equivalence of simulations in the canonical and grand canonical ensemble. Moreover, the canonical simulation gives indications for a cusp in $\langle\bar{\psi}\psi\rangle$ versus na^3 at $na^3 = 0.046$ (i.e. $B = 10$ on a 6^34 lattice). This is in good agreement with the results quoted in eq. (6.2) for the grand canonical ensemble.

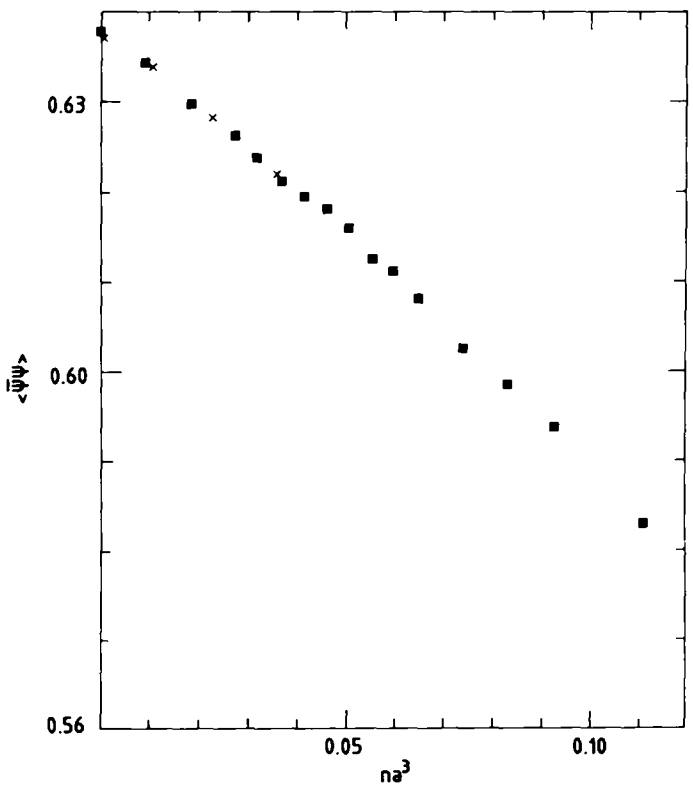

Fig. 10. As fig. 9 but on a 6^34 lattice (■). Some data from simulations with fixed chemical potential (×) on 8^34 lattices are also shown. Data points are based on 10^6 iterations.

7. Conclusions

We have studied the phase structure of strong coupling QCD at finite baryon-number density. Monte Carlo algorithms based on the MDP representation of the strong-coupling partition function turn out to be able to handle the remaining oscillations in the Boltzmann weights quite well. This enabled us to perform simulations both for the grand canonical ($\mu \neq 0$) and canonical ($B \neq 0$) ensembles.

We find evidence for a first-order phase transition at $\mu_c a = 0.63$. The critical baryon-number density turned out to be only slightly higher than ordinary nuclear-matter density. The analysis of the chiral condensate showed that chiral symmetry gets restored during this transition. It would be interesting to see whether this transition is also deconfining. For this purpose one needs the Polyakov loop expectation value $\langle L \rangle$ or the heavy-quark potential at finite density.

Quite contrary to standard simulations of QCD the measurement of observables depending on the quark fields (like $\langle \bar{\psi}\psi \rangle$ or hadron-hadron correlation functions) can be rather easily done in the MDP representation. On the other hand, the measurement of observables depending on the gauge fields (like Wilson and Polyakov loops) seems to be quite complicated in the MDP system, as these degrees of freedom have to be integrated out explicitly.

A preliminary and incomplete analysis of $\langle L \rangle$ indicates that it is large in the chiral-symmetric phase, which would mean that this phase is also deconfining. A more detailed analysis of this, as well as the temperature dependence of the transition, is planned for the future.

References

[1] F. Karsch, Z. Phys. C 38 (1988) 147
[2] F. Karsch and P. Hasenfratz, Phys. Lett. B125 (1983) 308
[3] A. Roberge and N. Weiss, Nucl. Phys. B275 [FS 17] (1986) 734;
D.E. Miller and K. Redlich, Phys. Rev. D35 (1987) 2524
[4] I. Barbour, N.E. Behilil, E. Dagotto, F. Karsch, A. Moreo, M. Stone and H. Wyld, Nucl. Phys. B275 [FS 17] (1986) 296
[5] G. Bhanot, S. Black, P. Carter and R. Salvador, Phys. Lett. B183 (1987) 331;
A. Gocksch, Phys. Rev. D37 (1987) 1014
[6] A. Gocksch, Phys. Rev. Lett. 61 (1988) 2054
[7] P. Rossi and U. Wolff, Nucl. Phys. B248 (1984) 105;
U. Wolff, Phys. Lett. B153 (1985) 92;
U. Wolff, Habilitationsschrift (Kiel, 1987)
[8] E. Dagotto, A. Moreo and U. Wolff, Phys. Rev. Lett. 57 (1986) 1292; Phys. Lett. B186 (1987) 395
[9] R.V. Gavai, Phys. Rev. D32 (1985) 519
[10] J. Engels and H. Satz, Phys. Lett. B159 (1985) 151
[11] P.E. Gibbs, University of Glasgow preprint, May 1986
[12] P.H. Damgaard, D. Hochberg and N. Kawamoto, Phys. Lett. B158 (1985) 239
[13] H. Kluberg-Stern, A. Morel and B. Petersson, Nucl. Phys. B215 [FS7] (1983) 527